An Optimal Control Approach for Plug-In Electric Vehicles in Active Distribution Systems Using Deep Reinforcement Learning

TAHIR, Yameena, NADEEM, Muhammad Faisal, RAZA, Muhammad Bilal and AKMAL, Muhammad <http://orcid.org/0000-0002-3498-4146>

IET Smart Grid

WILEY

The Institution of Engineering and Technology

ORIGINAL RESEARCH OPEN ACCESS

An Optimal Control Approach for Plug-In Electric Vehicles in Active Distribution Systems Using Deep Reinforcement Learning

Yameena Tahir[1] | Muhammad Faisal Nadeem[1] | Muhammad Bilal Raza[1] | Muhammad Akmal[2]

[1]Department of Electrical Engineering, University of Engineering and Technology (UET) Taxila, Taxila, Pakistan | [2]School of Engineering and Built Environment, Sheffield Hallam University, Sheffield, UK

Correspondence: Muhammad Akmal (m.akmal@shu.ac.uk)

Received: 29 July 2025 | **Revised:** 15 November 2025 | **Accepted:** 8 December 2025

Keywords: distribution networks | electric vehicles | learning (artificial intelligence) | optimal control

ABSTRACT

The penetration of plug-in electric vehicles (PEVs) and distributed energy resources (DERs) is increasing in distribution systems, potentially leading to significant technical and economic challenges. To tackle these challenges, this paper introduces a novel framework for effectively managing DERs and EVs within active distribution systems (ADSs), incorporating time-varying ZIP load models. A deep reinforcement learning (DRL)-based control approach is developed that simultaneously optimises both technical and economic objective functions for the efficient operation of ADSs. For this purpose, the PEVs are integrated with different nodes of the ADS through solid-state transformers (SSTs). Based on available generation, load demand and EV charging profiles, the control algorithm regulates reactive power flow using SSTs and minimises the operational cost as well as power loss of the ADS. The proposed framework is successfully applied and evaluated on standard IEEE systems, demonstrating its efficacy in solving the problem of integrating PEVs and DERs using solid-state transformers.

1 | Introduction

The high penetration and widespread integration of renewable energy-based distributed energy resources (DERs) are transforming power distribution systems from passive to active [1]. According to the U.S. Energy Information Administration (EIA), the share of U.S. electrical power generation from renewables is projected to rise from 21% in 2021 to 44% in 2050 [2]. In addition to the low emissions associated with renewable energy resources (RES), they may offer technical and economic benefits to distribution systems such as voltage regulation, improved power quality, enhanced system reliability, energy loss reduction and minimisation of operational cost [1, 3]. Apart from RES, plug-in electric vehicles (PEVs) have gained much attention due to their environmental and technological benefits. According to the International Energy Agency (IEA), the proportion of electric car sales has surged from 9% in 2021 to 14% in 2022, with a projected increase to 35% by 2030 [4].

In active distribution systems (ADSs), the high penetration of renewable energy-based DERs and PEVs can result in bidirectional power flow, leading to potential voltage excursions. One natural solution to address this issue is reactive power compensation. However, it may also increase reactive power flow and power losses in ADSs [5]. Furthermore, the uncoordinated charging and discharging of PEVs in ADSs, along with DERs and time-varying loads, may result in economic and energy losses. Therefore, a robust control strategy is required to simultaneously optimise the technical (voltage profile and power loss) and economic aspects of ADSs.

Over the years, an array of control techniques, including model predictive control [6], multi-timescale control [7], distributed optimal control [8] and coordinated volt-var control [9], have been presented for optimal voltage control in ADS. However, these methods are typically classified as model-based approaches, necessitating a mathematical model to depict voltage characteristics and power losses in ADSs. Although effective in optimising system voltages and minimising power losses, they depend heavily on comprehensive knowledge of the ADS, including active and reactive power injections and distribution line parameters. Such detailed information is often not readily accessible, posing challenges for accurate ADS modelling [10]. To address these limitations, control strategies based on reinforcement learning (RL) are being explored as a promising solution [11, 12].

At first, the Q-learning approach was utilised for the optimal control of shunt capacitors and tap-changing transformers. However, these traditional or non-SST-based voltage regulation methods lacked the dynamic reactive power management capabilities needed for ADSs [12]. Then, other RL techniques, such as batch RL [13] and multiagent RL [14], were utilised to resolve the voltage excursion and power loss issues. More efficient deep Q-learning algorithms were applied in many other studies [15, 16] for optimal voltage control in power systems. However, Q-learning and deep Q-learning cannot be simply implemented in continuous domains, and unfortunately, both the action and state spaces in voltage control problems are usually continuous [12–14]. Furthermore, the normal operation of ADSs requires different physical constraints to be satisfied, but conventional Q-learning techniques have limitations in systematically handling them [17]. To tackle these challenges, [18] introduced a constrained optimal control strategy based on the safe deep reinforcement learning (SDRL) algorithm for voltage control and loss reduction in ADSs through solid-state transformers (SSTs). In this control scheme, both action and statespaces are continuous, and information about the ADS dynamicmodel is unnecessary.

The literature highlights various control techniques that address technical challenges such as voltage violations and power loss arising from the presence of DERs and EVs in ADSs. However, to our knowledge, no existing methodology simultaneously addresses these technical issues while optimising system economics. Recent advancements in power electronics, particularly SSTs, offer high controllability for smooth voltage regulation and reactive power compensation. SSTs facilitate bidirectional power flow and efficient voltage control, making them ideal for integrating EV charging infrastructure into the grid. Additionally, their higher frequency results in reduced volume and weight compared to conventional transformers [19]. This makes them a top choice for charging stations in densely populated urban areas with high land costs, such as New York and California. Figure 1 compares conventional transformers and SSTs for EV charging infrastructure, clearly demonstrating the superiority of SSTs. As a result, this paper introduces SSTs, for the first time, for grid integration of EVs to control reactive power flows. The control algorithm regulates reactive power flow through SSTs and minimises the operational cost of ADSs based on the available generation (both from the grid and DERs), load demand and charging/discharging patterns of EVs. The original contributions of this paper are as follows:

1. For the first time, a robust framework for the optimum management of DERs is presented that includes PEVs in ADSs with time-varying *ZIP* load models.
2. The integration of EVs with ADSs through SSTs for improved reactive power optimisation and voltage regulation during grid-to-vehicle and vehicle-to-grid operation modes.
3. SDRL-based control strategy for the effective integration of PEVs in ADSs via SSTs while considering time-varying generation and load.
4. A centralised control approach for the simultaneous optimisation of technical and economic objective functions while PEVs are integrated with ADSs through SSTs.

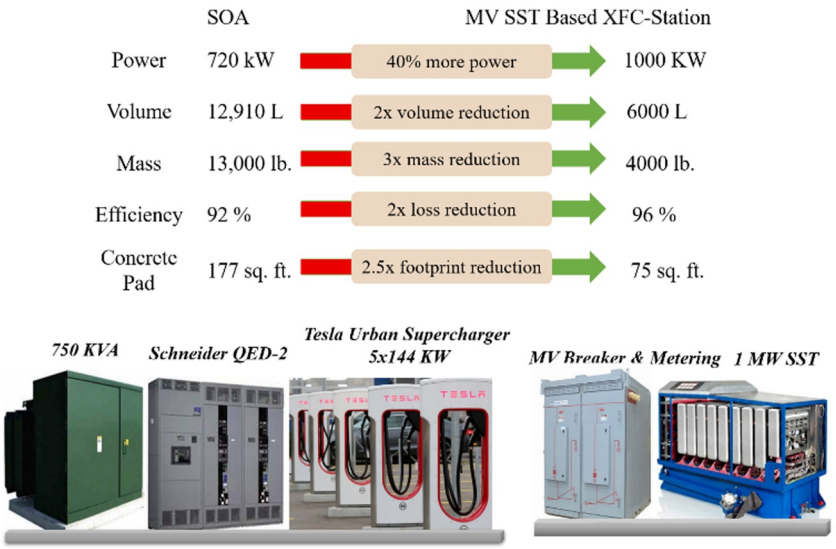

FIGURE 1 | Comparison of conventional and SST-based PEV charging.

2 | Framework and Modules of ADS

2.1 | Framework of ADS

The ADS framework in this research incorporates a standard distribution system linked with grid supply, DG units, PEVs and time-varying *ZIP* load models. DG units consist primarily of permanent magnet synchronous generators (PMSGs) operated via wind turbines. For optimal EV control in ADSs, SSTs are employed, capable of voltage conversion, energy transfer and reactive power compensation. The primary objective is to minimise ADS operational costs and power losses by maintaining bus voltages within allowable ranges using SSTs while considering time-varying *ZIP* load models. The single-line diagram of the ADS framework is shown in Figure 2. Specifically, N_W wind DGs and N_T SSTs are interconnected in the radial ADS. At the point of interconnection, the SST serves as a link between low- and medium-voltage levels.

2.2 | SST Modelling

The SST is fundamentally an AC/AC converter, also known as a power electronic transformer, that can replace the traditional low-frequency transformer in ADSs. The purpose of the SST is shaping the input current and offering bidirectional power flow accompanied by reactive power compensation [20] and harmonic elimination [21]. The topological structure of the SST considered in this research work is suitable for load flow computations and offers enhanced performance in the context of efficiency, size and weight [22]. As shown in Figure 3, it consists of three stages, that is, the medium-voltage (MV), isolation and low-voltage (LV) stages. The voltage source converter (VSC) at the MV stage initially converts incoming low-frequency AC voltage to DC and then converts it back to higher-frequency AC voltage. Similarly, the VSC at the LV stage of the SST converts high-frequency AC voltage into DC and then back into low-frequency AC voltage. The third stage involves a high-frequency transformer (HFT) that isolates the MV and LV stages.

The equivalent model of the SST is shown in Figure 4, where P_1 and Q_1 represent the active and reactive powers at the primary side, and P_2 and Q_2 represent the active and reactive powers at the secondary side. V_1 and V_2 are, respectively, the AC voltages at the MV and LV stages of the SST, V_0 and V_s represent the SST output voltage and system voltage, V_{dc} is the DC link voltage, and C is the capacitance of the DC link. x_1 and x_1 are the equivalent reactances on both sides of the SST. Furthermore, the modulation coefficients and the phase angles at the primary and secondary sides of the SST are represented by K_1, K_2, δ_1 and δ_2, respectively. The equations for V_{dc} and Q_1 at the primary side of the SST are as follows:

$$V_{\mathrm{DC}} = \frac{2P_1X_1}{K_1V_s \sin \delta_1}, \tag{1}$$

$$Q_1 = \frac{V_s(V_s - K_1V_{\mathrm{DC}} \cos \delta_1/2)}{X_1}. \tag{2}$$

The safe operation of the SST converter station with a fixed value is ensured by setting the values of δ_1 usually in the range $[-45°, 45°]$. Under such scenario, the partial derivatives of V_{DC} and Q_1 are given in the following equations:

$$\frac{\partial V_{\mathrm{DC}}}{\partial \delta_1} = -\frac{2P_1X_1 \cos \delta_1}{K_1V_s \sin^2 \delta_1}, \tag{3}$$

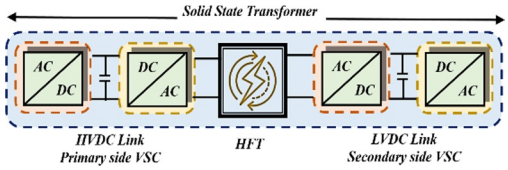

FIGURE 3 | Topology diagram of SST [23].

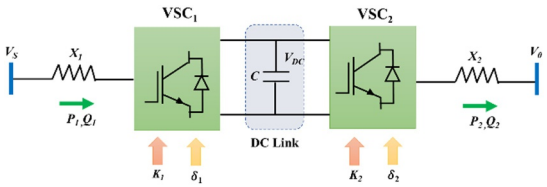

FIGURE 4 | Simplified model of SST [24].

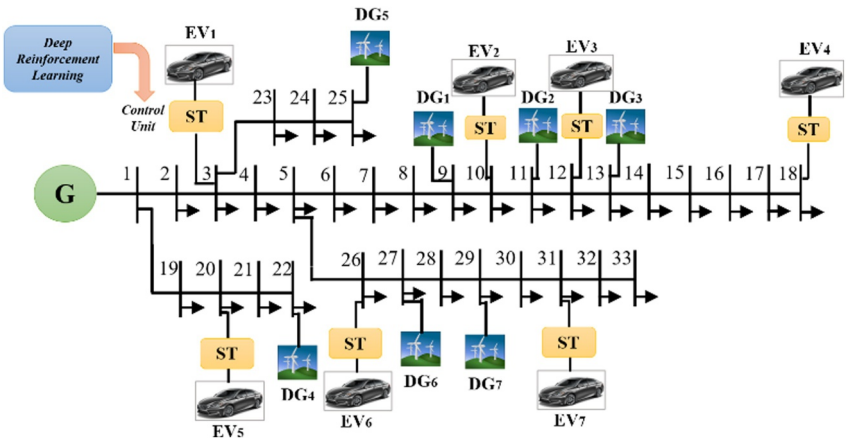

FIGURE 2 | Proposed framework of ADS.

$$\frac{\partial Q_1}{\partial K_1} = -\frac{V_{DC} V_s \cos \delta_1}{2X_1}. \quad (4)$$

The above equations demonstrate that $\partial V_{DC}/\partial \delta_1 < 0$ and $\partial Q_1/\partial K_1 < 0$. This implies that an almost similar functional relationship exists between V_{DC} and δ_1 as well as between Q_1 and K_1 that permits the decoupling control.

$$\Delta V_{DC} = W_{DC} \Delta \delta_1, \quad (5)$$

$$\Delta Q_1 = W_{q1} \Delta K_1, \quad (6)$$

where $W_{DC} = -\frac{2P_1 X_1 \cos \delta_1}{K_1 V_s \sin^2 \delta_1}$, $W_{q1} = -\frac{V_{DC} V_s \cos \delta_1}{2X_1}$

Therefore, V_{DC} and Q_1 can be controlled by tuning the δ_1 and K_1 parameters of the SST at the primary side. Likewise, the following equations of V_0 and Q_2 are formulated for the secondary side of the SST.

$$V_0 = \frac{2P_2 X_2}{K_2 V_s \sin \delta_2}, \quad (7)$$

$$Q_2 = \frac{V_0 (K_2 V_{DC} \cos \delta_2/2 - V_{0)}}{X_2}. \quad (8)$$

The partial derivatives of V_0 and Q_2 are as follows:

$$\frac{\partial V_0}{\partial \delta_2} = -\frac{2P_2 X_2 \cos \delta_2}{K_2 V_{dc} \sin^2 \delta_2}, \quad (9)$$

$$\frac{\partial Q_2}{\partial K_2} = -\frac{V_{dc} V_0 \cos \delta_2}{2X_2}. \quad (10)$$

The above equations demonstrate that $\partial V_0 / \partial \delta_2 < 0$ and $\partial Q_2 / \partial K_2 < 0$. Therefore, after decoupling, Equations (7) and (8) can be expressed as follows:

$$\Delta V_0 = W_v \Delta \delta_2, \quad (11)$$

$$\Delta Q_1 = W_{q2} \Delta K_2, \quad (12)$$

where $W_v = -\frac{2P_2 X_2 \cos \delta_2}{K_2 V_{dc} \sin^2 \delta_2}$, $W_{q1} = -\frac{V_{dc} V_0 \cos \delta_2}{2X_2}$

Therefore, V_0 and Q_2 can be controlled by tuning the δ_2 and K_2 parameters of the SST at the secondary side. Hence, the phase angles and modulation coefficients of the VSC on the primary and secondary sides of the SST are used as control parameters for reactive power compensation and voltage smoothing. Here, X_1 and X_2 represent the reactance at the primary and secondary converter sides of the SST. The above equations show that converter voltages and reactive power are updated by altering the values of the control parameters K_1, K_2, δ_1 and δ_2.

2.3 | Load Modelling

In this research work, time-varying ZIP load models are selected for the optimum management of DERs and PEVs in ADSs [25]. These load models are dependent on the node voltages and variable time, as shown in the following equations:

$$P(i,t) = P_0(i,t)\left[Z_p\left(\frac{V(i,t)}{V_0}\right) + I_p\frac{V(i,t)}{V_0} + P_p\right)\Bigg], \quad (13)$$

$$Q(i,t) = Q_0(i,t)\left[Z_q\left(\frac{V(i,t)}{V_0}\right) + I_q\frac{V(i,t)}{V_0} + P_q\right)\Bigg], \quad (14)$$

where V_0 denotes the ADS nominal voltage and $V(i,t)$ represents the voltage level of bus i at time t; $P(i,t)$ and $Q(i,t)$ are, respectively, the real power and reactive power demands of bus i at time t; and $P_0(i,t)$ and $Q_0(i,t)$ are the real power and reactive power demands of bus i at the nominal voltage V_0. The ZIP coefficients of active power are denoted by Z_P, I_p and P_p, whereas the *ZIP* coefficients of reactive power are denoted by Z_q I_q and P_q. This research assumes a normalised hourly load profile for three load types: residential, commercial and industrial, as provided in Ref. [26]. The ZIP coefficients for commercial, industrial and residential load models are obtained from Ref. [25].

2.4 | DG Modelling

The DG units in this study are wind turbines based on PMSGs. Wind speed data are sourced from the National Renewable Energy Laboratory (NREL) database [27]. A Weibull distribution-based probabilistic generation model is used to calculate the output power of the wind turbine [26].

$$f_{(t)}(v_{(t)}) = \left(\frac{k_{(t)}}{v_{(t)}}\right)\left(\frac{v_{(t)}}{c_{(t)}}\right)^{k_{(t)}-1} e^{\left(-\left(\frac{v_{(t)}}{c_{(t)}}\right)^{k_{(t)}}\right)}, \quad (15)$$

where $v_{(t)}$ is the wind speed and $k_{(t)}$ represents the shape parameter, whereas $c_{(t)}$ is the scale factor at time step 't'. Depending upon the hourly wind speed data, the active power output of wind DG, shown in Figure 5, is computed using the following function [26]:

$$P_{WT} = \begin{cases} 0 & v < v_{ci} \text{ or } v > v_{co} \\ \dfrac{P_R \times v}{v_R - v_{ci}} - v_{ci} & v_{ci} \le v < v_r \\ P_R & v_R \le v < v_{co} \end{cases}, \quad (16)$$

where P_R represents the rated capacity; and v_{ci}, v_{co} and v_R are the cut-in, cut-out and rated speeds of the PMSG, respectively.

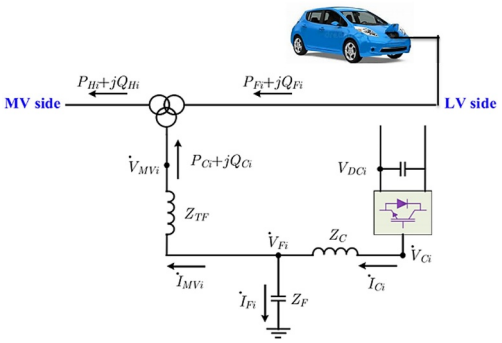

FIGURE 5 | Equivalent circuit of SST employed with EV.

2.5 | Plug-In Electric Vehicle

In this paper, PEVs are integrated with ADSs through SSTs for reactive power support, bidirectional power flow and energy storage [23]. Furthermore, this compensates for the uncertainty imposed by the RES integration in the ADS by controlling the charging and discharging strategies of EVs. The design of the SST employed with EVs used in the system is shown in Figure 5. The mathematical model of the PEV state of charge (SOC) is given in the following equation [28, 29]:

$$\mathrm{soc}^{t}_{\mathrm{PEV}s}=\begin{cases} E^{\mathrm{PEV}}_{\mathrm{Int}}+\sum_{j=1}^{t}\left(\mu^{\mathrm{PEV}}_{\mathrm{Chr}}\times P_t^{\mathrm{PEV}_{\mathrm{chr}}}-\dfrac{P^{\mathrm{PEV}_{\mathrm{disch}}}}{\mu^{\mathrm{PEV}}_{\mathrm{disch}}}\right), \forall t\le d-1 \\ E^{\mathrm{PEV}}_{\mathrm{Int}}+\sum_{j=1}^{t}\left(\mu^{\mathrm{PEV}}_{\mathrm{Chr}}\times P_t^{\mathrm{PEV}_{\mathrm{chr}}}-\dfrac{P^{\mathrm{PEV}_{\mathrm{disch}}}}{\mu^{\mathrm{PEV}}_{\mathrm{disch}}}\right)-E^{t}_{\mathrm{out}}, \\ \forall t\ge f+1 \end{cases} \tag{17}$$

$$Pk^{\mathrm{PEV}}_{\mathrm{minimum}}\le\ Pk^{\mathrm{PEV}}_{\mathrm{Chr/disch.}}\ \ge Pk^{\mathrm{PEV}}_{\mathrm{maximum}},$$

$$E^{\mathrm{PEV}}_{0}=E^{\mathrm{PEV}}_{24},$$

$$E^{\mathrm{PEV}}_{d-1}=E^{\mathrm{PEV}}_{\mathrm{maximum}}.$$

The PEV charging/discharging is influenced by both DER generation and the network's demand requirements. PEVs can interact with the electrical grid in two ways: (1) storing low-cost energy during off-peak hours to act as an energy storage device and (2) discharging the stored energy during peak hours to serve as a cost-effective energy source. The following equation determines the optimal charging/discharging profile of PEVs.

$$P^{\mathrm{demand}}+\sum_{n=1}^{N_{\mathrm{PEV}}}P_n^{\mathrm{PEV}_{\mathrm{Chr}}}+P_L=P^{\mathrm{grid}}+\sum_{n=1}^{N_{\mathrm{PEV}}}P_n^{\mathrm{PEV}_{\mathrm{disch}}}+P_{\mathrm{WT}}\,. \tag{18}$$

PEV charging/discharging cost is calculated as follows [30]:

$$\mathrm{Cost}^{h}_{\mathrm{PEVs}}=\begin{cases} \sum_{j=1}^{\mathrm{NPEVs}}\sum_{h=1}^{24}\beta\times \mathrm{PEV}_{j,h}^{\frac{\mathrm{Charging}}{\mathrm{Discharging}}}+ \\ \left(\mathrm{PEV}_{j,h}^{\mathrm{Charging}}\times R^{\mathrm{Charging}}-\mathrm{PEV}_{j,h}^{\mathrm{Discharging}}\right. \\ \left.\times\kappa^{\mathrm{Dischargingh}}\right) \end{cases}, \tag{19}$$

where $\kappa^{\mathrm{Dischargingh}}$ and β are operation coefficients of PEVs.

3 | Control Problem Formulation

3.1 | Optimal Voltage Control Problem

The ADS considered in this research for the investigation of hosts' B_n buses is shown in Figure 2, illustrating its radial network topology as a connected tree. The edge set in the tree is represented by ε, where $(m, n)\in\varepsilon$ if the ADS bus m is connected to n.

Consider $V_m=|V_m|$, where m represents the voltage at bus m, and then gather all the network voltages to form $V=\left[V_1, V_2, ..., V_{B_N}\right]^T$. Similarly, at bus m, the active and reactive powers are denoted by P_m and Q_m and are combined in two vectors, $P_m=[P_1,\ P_2, ..., P_{B_N}]$ and $Q_m=[Q_1,\ Q_2, ..., Q_{B_N}]$, respectively. Furthermore, the combination of the SST controllable reactive powers Q_{cm} and the change in them ΔQ_{cm} is represented by the vectors $Q_C=\left[Q_{C1}, Q_{C2}, ..., Q_{CB_N}\right]^T$ and $\Delta Q_C=\left[\Delta Q_{C1}, \Delta Q_{C2}, ..., \Delta Q_{CB_N}\right]^T$. The admittance matrix is denoted by $\mathbf{Y}$, and the admittance of the line (m, n) is represented by $y_{mn}=g_{mn}+jb_{mn}$. These representations are used to write the following equations of ADS power flow.

$$P+j(Q+Q_C+\Delta Q_C)=\mathbb{R}e\{\mathrm{diag}(VV^HY^H)\}+Im\{\mathrm{diag}(VV^HV^H)\}, \tag{20}$$

where diag(.) gathers the diagonal of a square matrix, and the Hermitian transpose of $V(Y)$ is V^HY^H. The active power flow via ADS can be calculated as follows:

$$P_{mn}=|V_m|^2g_{mn}+|V_m||V_n|\left[b_{mn}\sin(\delta_{mn})-g_{mn}\cos(\delta_{mn})\right], \tag{21}$$

where $\delta_{mn}=(\delta_m-\delta_n)$. Using Equation (21), the overall power loss in ADS is calculated as follows:

$$P_L=\sum_{m,n:(m,n)\in\varepsilon}P_{mn}+P_{nm}. \tag{22}$$

The main aim of this research is to regulate voltage within permissible limits at each ADS bus while minimising operational costs and power losses. SSTs are utilised to shape reactive power injection profiles, facilitating voltage control across the ADS. Consequently, the optimal voltage control problem is formulated as an optimisation programme.

$$\min\ \xi P_L(Q_C+\Delta Q_C)+(1-\xi)\|\Delta Q_C\|^2. \tag{23}$$

The parameter ξ typically ranges from 0.1 to 0.9. However, in this framework, it is set to 0.7 to strike a balance between reducing power losses and minimising control effort [18].

Subject to:

Voltage magnitude constraint

$$V_{\min}\le|V_m|\le V_{\max},\ m=1, 2, ..., B_N. \tag{24}$$

Power handling constraint

$$P+j(Q+Q_C)=\mathbb{R}e\{\mathrm{diag}(VV^HY^H)\}+Im\{\mathrm{diag}(VV^HV^H). \tag{25}$$

SST power constraints

$$\begin{cases} P_1=P_2 \\ S\ge\sqrt{P_1^2+Q_1^2} \\ S\ge\sqrt{P_2^2+Q_2^2} \end{cases}. \tag{26}$$

SST control constraints

$$\Delta Q_{Cm}(k) \geq Q_{C,\min}(P_{Cm}(k)) - Q_{Hm}(k-1) + Q_{Fm}(k), \quad (27)$$

$$\Delta Q_{Cm}(k) \leq Q_{C,\max}(P_{Cm}(k)) - Q_{Hm}(k-1) + Q_{Fm}(k). \quad (28)$$

The optimisation problem in Equation (23) is difficult to solve directly due to two reasons. Primarily, it is nonconvex because of the nonlinear relationship between ADS power and bus voltages, and secondly, the **Y** parameters of the ADS are fundamentally not certain and therefore may not be simply available. The following section addresses these challenges by formulating the optimisation problem as a constrained Markov decision process (CMDP), followed by applying the SDRL approach to solve the problem.

3.2 | Optimal Voltage Control as CMDP

The optimum voltage control problem necessitates real-time reactive power dispatch in the ADS. The proposed control strategy must coordinate with all ADS SSTs to meet voltage constraints and minimise operational costs and power losses. This problem involves all components of CMDP, where the agent's actions affect the environment's states. The agent's goal is to devise the most favourable policy, maximising rewards while minimising power losses. Specifically, the policy involves the interaction of ADS states with SSTs for reactive power adjustments, as depicted in Figure 2. Because this paper treats the optimum voltage control problem of ADS as a CMDP, it requires three parameters: states (S), actions (A) and rewards (R). The states represent a real-time measure of the environment or the evolution of system dynamics. For the case of ADSs and SSTs, the dynamics of the system are continuous. Therefore, to fully characterise the continuous nature of the ADS, the system states are represented as continuous variables. The states are defined as the voltage magnitudes of all buses in the ADS.

$$\mathrm{S} = \left[|V_1|, |V_1|, \ldots |V_{B_N}|\right]. \quad (29)$$

The second parameter is the set of actions, which, in the case of ADS, is considered as reactive power adjustments.

$$\mathrm{A} = [|\Delta Q_1|, |\Delta Q_2|, \ldots |\Delta Q_{\mathrm{SST}}|]. \quad (30)$$

The action vector comprises continuous variables, resembling the characteristics of states. Thus, we introduce the voltage control policy denoted by $\gamma(.)$ to map actions and states.

$$a_t = \gamma(s_t). \quad (31)$$

At each time step t, every element of the action vector a_t is constrained by the reactive power limits of the SST. The reward 'r' is directly related to the control strategy's goals and is formulated as the negative of the overall power loss in the ADS, with an added penalty for control effort, aiming to minimise power losses and operational costs.

$$R = -\beta P_L\,(Q_i + \Delta Q_i) - (1-\beta)\,|\Delta Q_i|^2. \quad (32)$$

The reduced reward from time t onwards is denoted by r_t and is typically called the return.

$$r_t = \sum_t^{\infty} \gamma^{\{\tau - t\}} r_t \quad (33)$$

The function of the action value, also known as the Q function, represents the expected return at state s_t and action a_t under the control policy γ:

$$Q^{\gamma}(s_t, a_t) = E(r_t | s_t, a_t; \gamma) \quad (34)$$

The optimum voltage control problem in ADS evolves into maximising the performance function through determining γ.

$$J(\gamma) = E(r_t; \gamma). \quad (35)$$

The line parameters and active and reactive power injections are not known during the actual operation of the ADS; therefore, it is not possible to derive the transition model. Consequently, a DRL approach is adopted for solving the CMDP because it does not require a definite transition model [18].

4 | Safe Deep Reinforcement Learning for ADS Optimal Voltage Control

In this study, the deep deterministic policy gradient (DDPG) algorithm is employed to learn the policy γ for optimal voltage control in ADS, as outlined in Algorithm 1. Here, the control policy γ is constrained by a vector δ^{γ}, indicating that learning γ essentially involves discerning optimal values for δ^{γ}. In policy gradient methods, such as DDPG, suboptimal values of δ^{γ} are learnt, with DNNs approximating both the critic and the actor [18]. To maximise $J(\gamma)$, the direction of δ^{γ} has an important role. The derivative of $J(\gamma)$ with respect to δ^{γ} is termed the action gradient and is expressed as follows:

$$\nabla \delta^{\gamma} J(\gamma) = \mathbb{E}[\nabla_a Q(s,a) \nabla_{\delta^{\gamma}} \gamma(s)]. \quad (36)$$

The performance function J varies with the change in Q, which is unknown and therefore required to be approximated. To do this, an actor–critic-based framework is utilised by DDPG, which is explained in Algorithm 1. The actor approximates the control policy, whereas the critic is utilised to approximate function Q. With robust learning capabilities, two DNNs are used to formulate the actor and critic networks. These networks, constrained by vectors δ^{Q} and δ^{γ}, represent the Q function and the voltage control policy, respectively [31]. Policy gradient methods learn these constraint vectors. DDPG employs target networks to facilitate smooth learning, with target actor and critic networks tracking the main networks' constraints steadily. These networks derive target values, with their constraint vectors steadily tracking the critic and actor networks, as shown in the following equations:

$$\delta^{Q'} = \rho \delta^{Q} + (1-\rho)\delta^{Q'}, \quad (37)$$

$$\delta^{\gamma'} = \rho \delta^{\gamma} + (1-\rho)\delta^{\gamma'}, \quad (38)$$

where ρ, a positive number, is significantly smaller than 1. This ensures that the target parameters change gradually,

significantly improving the smooth progress of the DDPG learning process. An obstacle in using reinforcement learning with DNNs is that many optimisation methods assume samples are identically and independently distributed, which is invalid when samples are obtained through sequential exploration, such as in voltage control in ADS. To address this, DDPG constructs a replay buffer filled with transition samples. For each time interval, critic and actor values are obtained by uniformly sampling a subset of training data from the buffer. As DDPG is not an online learning method, the buffer size may be large, allowing DDPG to learn from uncorrelated transitions. The DDPG learning approach for optimal voltage control in ADS is detailed in Algorithm 1. The critic network δ^Q should be updated to minimise the loss function, as given in the following equation:

$$\frac{1}{R}\sum_{m=1}^{R}[r_m + \varphi Q'(S_{m+1}, \gamma(S_{m+1} - Q(S_m, a_m)]^2, \tag{39}$$

where the replay buffer size is denoted by 'R'. Similarly, the actor network δ^γ should be updated to maximise the performance function $J(\gamma)$. The direction of update can be determined using the following expression:

$$\nabla\delta^\gamma J(\gamma) \approx \frac{1}{R}\sum_{m=1}^{R}\nabla_a Q(S_m, \gamma(S_i))\,\nabla_\delta^\gamma\,\gamma(S_m). \tag{40}$$

ALGORITHM 1 | Safe Deep Deterministic Policy Gradient (DDPG).

Initialize critic network Q(s,a|θ^Q) and actor network μ(s|θ^μ) with random weights.
Initialize target networks Q′ and μ′ with θ^{Q′} ← θ^Q, θ^{μ′} ← θ^μ.
For episode = 1 to M:
  Initialize a random process $\mathcal{N}$ for exploration.
  Receive initial observation state s_1.
  For t = 1 to T:
    Select action a_t = μ(s_t|θ^μ) + $\mathcal{N}$_t.
    Apply action constraints:
      a_ti = max(a_ti, Q_{C,max} (P_Ci(t) − Q_Hi(t−1) + Q_Fi(t)))
      a_ti = min(a_ti, Q_{C,min} (P_Ci(t) − Q_Hi(t−1) + Q_Fi(t)))
    Correct the action a_t using the safety layer (Eq. 44).
    Execute a_t, observe reward r_t and next state s_{t+1}.
    Store transition (s_t, a_t, r_t, s_{t+1}) in replay buffer $\mathcal{R}$.
    Sample a random minibatch of N transitions from $\mathcal{R}$.
    Set target value:
      y_i = r_i + γ Q′(s_{i+1}, μ′(s_{i+1}|θ^{μ′})|θ^{Q′})
    Update critic by minimizing:
      L = (1/N) Σ (y_i − Q(s_i, a_i|θ^Q))²
    Update actor using the policy gradient.
    Update target networks using soft updates.

The critic network features 8 hidden layers, including 4 ReLU and 3 fully connected layers, whereas the actor network comprises 6 hidden layers, including 2 ReLU and 3 fully connected layers. Additionally, to prevent voltage profile violations, a safety layer is introduced. The proposed framework algorithm seamlessly operates on continuous action and state spaces, reflecting voltage control in the ADS via SSTs.

4.1 | Handling Constraints Using Safety Layer

This paper employs a sensitivity matrix-based technique to address ADS voltage constraints. In this approach, the voltage state is modelled in relation to action using a first-order mathematical expression, as shown below:

$$s_{t+1,n} = s_{tn} + w(s_{tn};\ \delta_n^w)a_t,\ n = 1, 2, ..., B_N, \tag{41}$$

where w denotes the mapping function that considers s_{tn} as input and $s_{t+1,n}$ as the output vector that has an identical dimension to a_t . The analysis of above function, in view of ADS, shows that the mapping function w is fortuitously similar to the sensitivity matrix S_i, which illustrates the change in bus voltages after taking control actions, as follows:

$$S_i = \begin{bmatrix} \frac{\partial V_1}{\partial Q_{C1}} & \cdots & \frac{\partial V_1}{\partial Q_{CN_T}} \\ \vdots & \ddots & \vdots \\ \frac{\partial V_{B_N}}{\partial Q_{CN_T}} & \cdots & \frac{\partial V_{B_N}}{\partial Q_{CN_T}} \end{bmatrix}. \tag{42}$$

The sensitivity matrix S_i is computed using the transposed inverse of the Jacobian matrix used in power flow [6]. Subsequently, an additional safety layer is embedded in the output layer (maps state with action) of the DDPG actor network. The main purpose of the safety layer is constraint handling during the solution of optimisation problems.

$$\min_{a_t}\ \frac{1}{2}\|a_t - \gamma(s_t)\|^2. \tag{43}$$

Subject to

$$s_{tm} + S_m a_t \le V_{\max},\ m = 1, 2, ..., B_N,$$

$$-s_{tm} - S_m a_t \le -V_{\max},$$

$$m = B_N + 1, ...2B_N.$$

The analytical solution of Equation (41) may be simply computed using the following equation:

$$a_t^* = \gamma(s_t) - \mu_n^* S_i^T, \tag{44}$$

where

$$\mu_j = \left[\frac{S_i\gamma(s_t) + s_{tn} - (V_{\max} - \sigma)}{S_i S_i^T}\right]^+ m = 1, 2, ..., B_N, \tag{45}$$

$$\mu_j^* = -\left[\frac{-S_i\gamma(s_t) - s_{tn} + (V_{\max} + \sigma)}{S_i S_i^T}\right]^+, m = 1, 2, ..., 2B_N, \tag{46}$$

where [.]* represents the operation max, and μ_j^* is the Lagrange multiplier corresponding to the jth constraint [18]. By adjusting the action a_t using Equation (44), the voltage violation in Equation (24) can be eliminated.

5 | Numerical Simulations

The proposed work presents an SDRL scheme for the optimal control of PEVs in ADSs. This scheme enables multiple SSTs integrated with PEVs to participate in ADS control for reactive power compensation for time-varying *ZIP* loads. The hourly demand patterns of all load models are obtained from Ref. [26]. It is supposed that in the case of all load types, the load connected to each bus of the ADS is of the same type; that is, while studying the residential time-varying *ZIP* load model, the load connected to each bus is of the residential type, and the same applies for the other load models. The utilisation of the DDPG algorithm allows the achievement of both system power loss reduction and voltage regulation. Training of the DDPG agent is performed using the RL Toolbox in MATLAB 2021a. The parametric settings employed during the training are shown in Table 1. Moreover, all hyperparametric values, such as the number of neurons for each layer, are selected based on common practices [11] and are finely turned using a trial-and-error method.

5.1 | Case Study

The effectiveness of the proposed approach is verified through implementation on both IEEE 33-bus and 69-bus systems [26]. Within the system, N_{DG} signifies the number of DG units, specifically denoting the use of permanent magnet synchronous generators in wind turbines. Notably, the SST's output power and voltage are continuously adjustable. For the 33-bus system, seven DG units are integrated with buses 9, 11, 13, 22, 25, 27 and 29, whereas an additional seven SSTs are integrated with PEVs at buses 3, 10, 12, 18, 20, 26 and 31, respectively. In the case of the 69-bus system, a total of 10 DG units are integrated at buses 9, 5, 8, 15, 20, 25, 32, 36, 45, 54 and 62. Additionally, there are 9 SSTs integrated with EVs installed at buses 4, 9, 24, 28, 30, 34, 53, 61 and 69. In this context, the SSTs collaborate with the EVs to mitigate uncertainties arising from RESs. Different multipliers are applied to the original time-varying ZIP load model data to ensure diverse load profiles among the buses. A 20% Gaussian noise is incorporated to simulate stochastic uncertainty.

TABLE 1 | Summary of algorithmic parametric settings.

Items	Value
Sampling time	10 s
Smoothing factor	0.001
Experience buffer	10^5
Discounting factor	0.95
Minibatch size	128
Max episode	10^4
Critic learning rate	0.001
Critic regularisation factor	10^{-4}
Actor learning rate	0.001
Actor regularisation factor	10^{-4}
Tighten margin	0.05
$V_{\max}$	1.05 p.u.
$V_{\min}$	0.95 p.u.

To demonstrate the learning capability of the proposed safe DRL framework, we have conducted a series of experiments that span deterministic and stochastic policy-based strategies. Our training process comprises 300 days of dataset, with the parametric configuration being in Table 1. The simulation results obtained from the trained model across the proposed networks are shown in Figure 6. In this figure, the reward, power losses and voltage violation rates indicate the daily accumulated values. During the training phase, particularly between Days 20 and 50, as shown in Figure 6, the Safe-DDPG demonstrates better convergence compared to its state-of-the-art standard counterparts, that is DDPG, SAC and TD3. Furthermore, the analysis based on 250 and 300 days exhibits that Safe-DDPG shows higher reward and improved voltage and power loss mitigation compared to DDPG, SAC and TD3, as supported by the results in Table 2. The findings demonstrate that the proposed Safe-DDPG achieves mean episodic rewards of −2.603 and −3.943 on the IEEE 33-bus and 69-bus networks, indicating the improvements of 30.2% and 28.0%, respectively, over standard DDPG and highlighting that the safety layer significantly increases the average episodic reward while lowering the rate of voltage violation, thereby affirming operational safety. Moreover, these improvements remain consistent when compared to TD3 and SAC baselines. Hence, the results confirm that each design element, particularly the inclusion of the safety layer and SST mapping, significantly enhances the learning process by ensuring safety and effective learning behaviour.

5.1.1 | No Control Case

The hourly voltage profile at the buses of both ADSs, for all time-varying *ZIP* load models without any voltage control or PEV integration, is illustrated in Figures 7 and 8. Two overvoltage periods can be observed for both the 33-bus and 69-bus ADSs. In the case of the 33-bus system, these periods occur from 2 to 4 AM and from 11 AM to 2 PM. For the 69-bus system, the first overvoltage period occurs in the morning when the load is low and DGs operate at maximum capacity, and the second occurs around mid-day when DG generation peaks. These overvoltage periods occur due to relatively low demand compared to the availability of wind generation. As expected, the most problematic voltage deviations occur at buses where DGs are installed. Undervoltage can be observed during the late hours when demand is high, whereas generation is low. Moreover, there are also instances of undervoltage occurring when demand is high, but DG's output is relatively low.

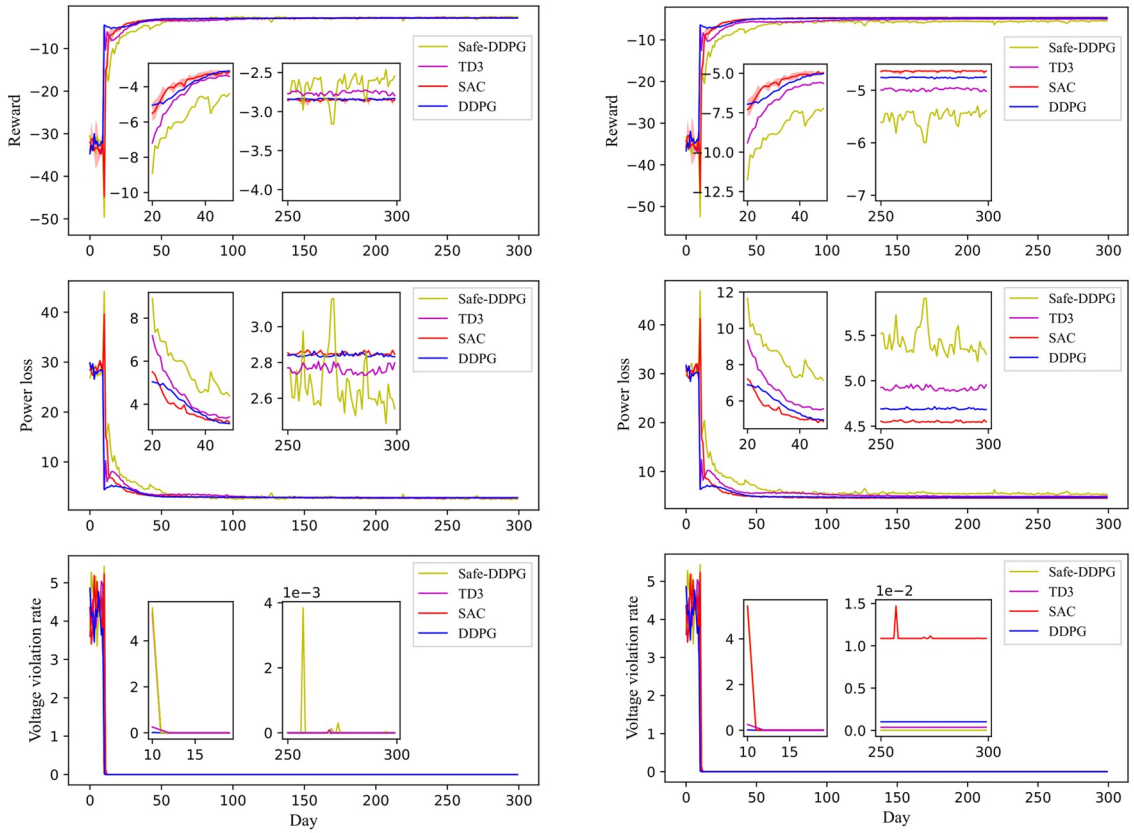

FIGURE 6 | Simulation results and comparative analysis with and without safety layer learning approaches.

TABLE 2 | Simulation results and comparative analysis of IEEE 33-bus and 69-bus systems.

	Reward		Power losses (MW)		Voltage violation rate	
Algorithm	**33-bus**	**69-bus**	**33-bus**	**69-bus**	**33-bus**	**69-bus**
Safe-DDPG	−2.603	−3.943	2.6031	3.942	$4.317e^{-6}$	$5.172e^{-5}$
TD3	−2.849	−4.597	2.8471	4.596	$5.231e^{-5}$	$7.246e^{-4}$
SAC	−3.067	−4.917	3.0671	4.916	$1.459e^{-5}$	$7.96e^{-2}$
DDPG	−3.727	−5.473	3.7262	5.426	$8.639e^{-5}$	$1.246e^{-4}$

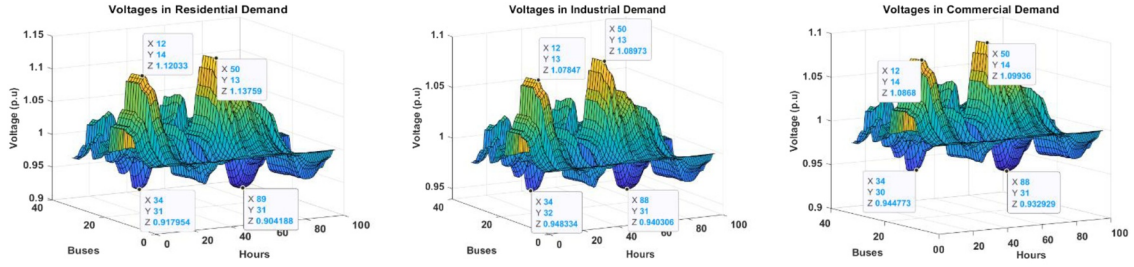

FIGURE 7 | Voltage profiles of 33-bus ADS without voltage control.

5.1.2 | Control Case Without PEV

First, results are obtained without considering the variable EV schedule illustrated in Figures 9 and 10. Notably, when a substantial amount of active power is supplied by DG units to the system, voltages at all bus locations tend to rise, leading SSTs to absorb reactive power during this period. Conversely, during periods of low wind when DG output is minimal, voltages at all buses tend to decrease, prompting SSTs to inject reactive power to support the system voltage. This control mechanism ensures voltage stability at all buses of the ADS, including the critical buses where DGs are installed, as shown in Figure 2, effectively

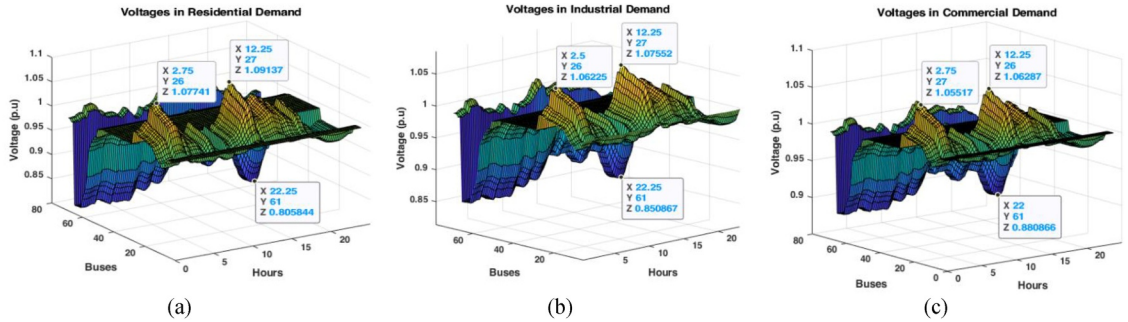

FIGURE 8 | Voltage profiles of 69-bus ADS without voltage control.

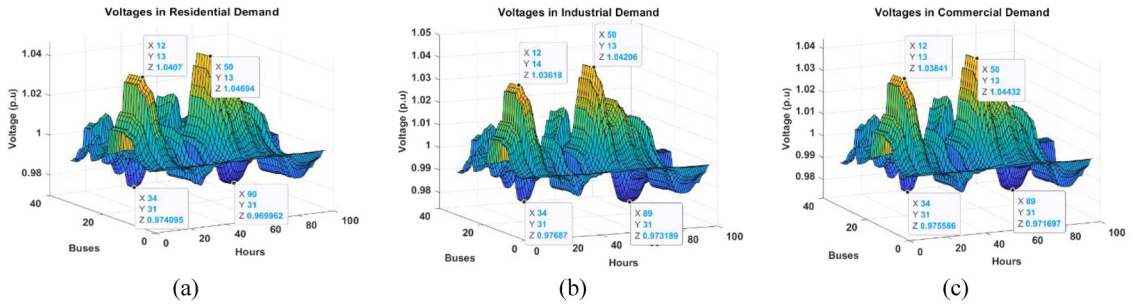

FIGURE 9 | Voltage profiles of 33-bus ADS without EV scheduling.

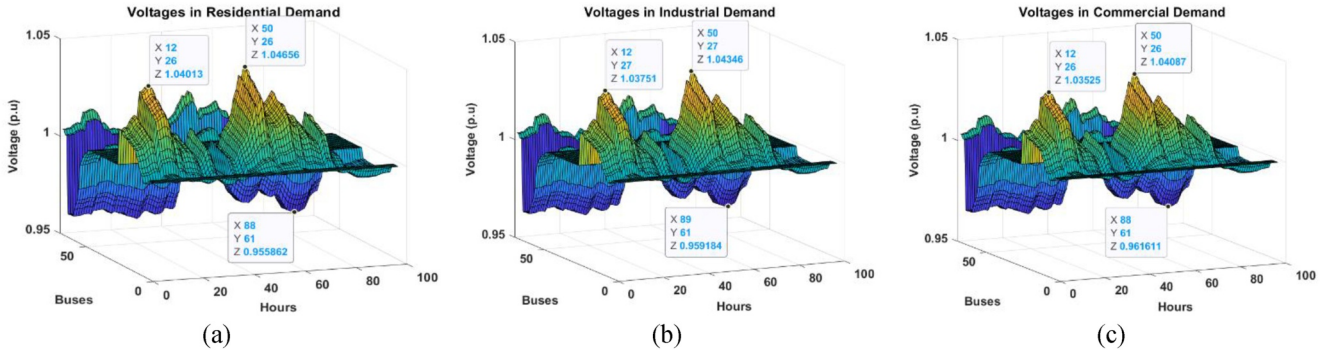

FIGURE 10 | ADS voltage profiles under the proposed scheme without EV scheduling.

maintaining them within the desired range. These findings affirm the capability of the proposed SDRL scheme to handle constraints. Simulation results indicate that the most improved per-unit voltage profile is observed for residential load types, followed by commercial and industrial types.

5.1.3 | Control Case With PEVs

5.1.3.1 | Technical Analysis. The charging/discharging pattern of PEVs is determined through Equation (18) and is presented in Figure 11. Considering this PEV schedule, the voltage profile results of both 33- and 69-bus ADSs for all load types are shown in Figures 12 and 13.

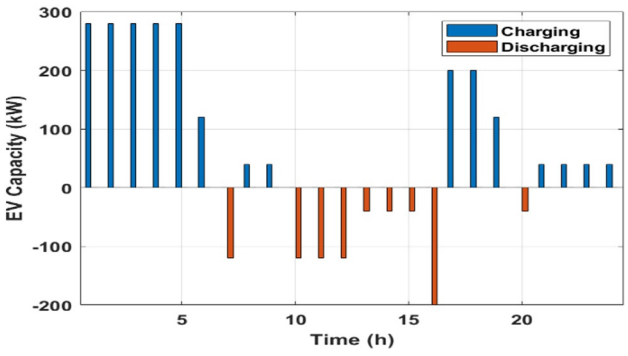

FIGURE 11 | Daily charging/discharging schedule of EVs.

The outcomes underscore the robust performance of the SDRL-based control approach. Recognising that abrupt shifts in power demand and the escalating presence of PEVs in ADSs can impact system performance, it becomes crucial to ensure that DERs' output and the charging/discharging patterns of PEVs align with the time-varying characteristics of the ADS to effectively mitigate renewable-related uncertainties. In Figure 14, the daily evolution of reactive power for the seven SSTs, representing control actions, is shown. The trained agent drives SSTs to absorb reactive power during voltage swells, restoring

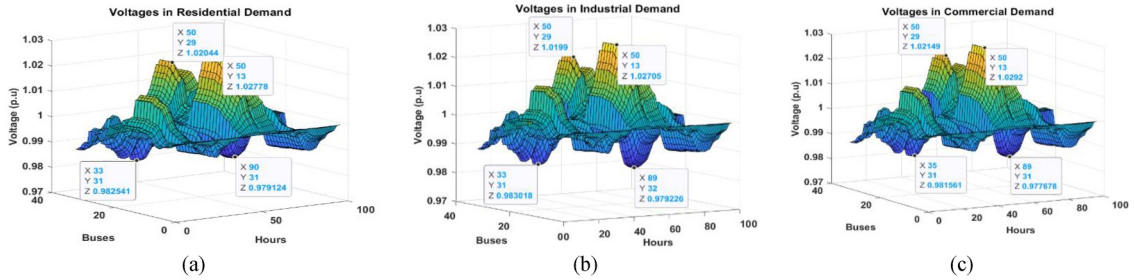

FIGURE 12 | Voltage profiles of 33-bus ADS with EV scheduling.

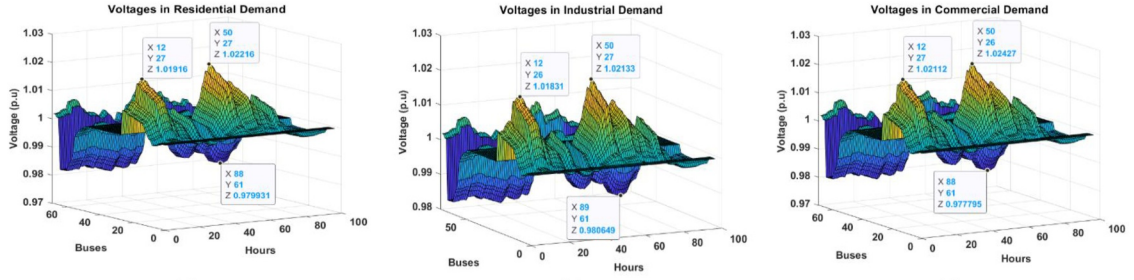

FIGURE 13 | ADS voltage profiles with EV scheduling.

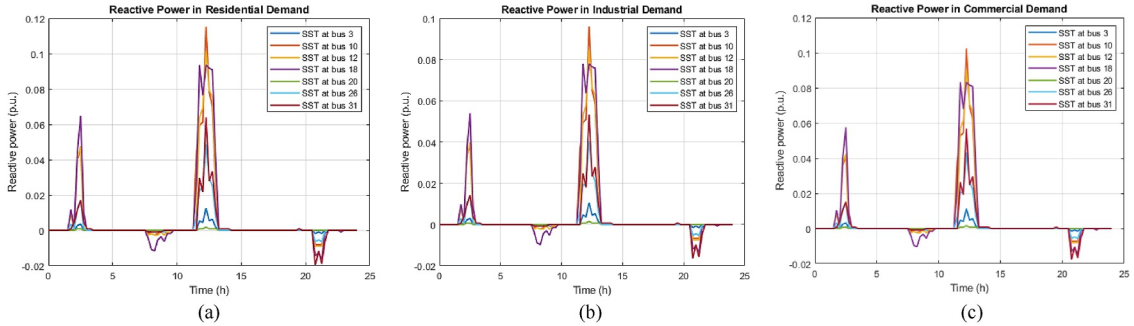

FIGURE 14 | Hourly SST reactive power in all TVVD.

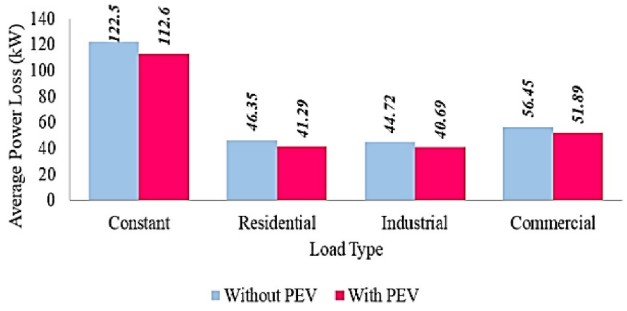

FIGURE 15 | 33-bus ADS loss comparison with and without PEVs.

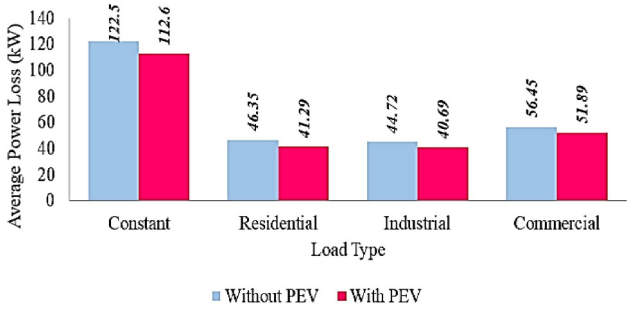

FIGURE 16 | 69-bus ADS loss comparison with and without PEVs.

voltages within acceptable limits and facilitating power transfer to the LV side for PEV charging. Conversely, during voltage sags, SSTs inject reactive power, rectifying voltages within specified limits and enabling power transfer from PEVs to the grid for discharge. Furthermore, the results for average power loss of ADSs in the case of each time-varying *ZIP* load model with and without integration of PEV are presented in Figures 15 and 16. The results demonstrate that the integration of PEV with the proposed voltage control framework has a significant impact on the reduction of average power losses in the case of all time-varying *ZIP* load models for residential load type, followed by commercial and industrial load types, respectively.

5.1.3.2 | Economic Analysis. The results obtained indicate that the incorporation of PEVs through SSTs using the proposed control framework into ADSs with time-varying ZIP load models has a substantial influence on reducing overall generation expenses, as illustrated in Table 3. The most significant cost

TABLE 3 | Cost analysis of different load models with and without PEVs.

ADS	Load type	Cost ($)		
		No EVs	With EVs	% reduction
33-bus	Residential	907	698	23.05
	Industrial	718	501	30.23
	Commercial	963	752	21.92
69-bus	Residential	959.46	750.46	21.79
	Industrial	770.46	553.46	28.17
	Commercial	1015.46	804.46	20.78

reduction is observed in the case of time-varying industrial load models, followed by residential and commercial models.

6 | Conclusion

In conclusion, this paper proposes a novel framework utilising DRL for the effective management of DERs and PEVs within ADSs. The incorporation of time-varying ZIP load models makes the framework outcome more realistic, enabling a more comprehensive optimisation of both technical and economic objectives. Through the integration of PEVs at different nodes of the ADS using SSTs, the developed control approach successfully regulates reactive power flow based on available generation, load demand and charging/discharging patterns. The application of the proposed framework to standard systems demonstrates its efficacy in addressing the challenges associated with the increasing penetration of PEVs and DERs. By simultaneously minimising operational costs and power losses, this approach proves to be a valuable contribution to the efficient operation of distribution systems in the face of evolving energy landscapes. As the energy transition continues, the presented framework offers a promising solution for the sustainable and optimal integration of renewable energy sources and electric vehicles into distribution networks.

Author Contributions

Yameena Tahir: conceptualization, data curation, investigation, software, writing – original draft. **Muhammad Faisal Nadeem:** conceptualization, data curation, formal analysis, investigation, methodology, project administration, resources, software, supervision, validation, visualization, writing – review and editing. **Muhammad Bilal Raza:** formal analysis, validation, visualization, writing – original draft. **Muhammad Akmal:** supervision, writing – review and editing.

Funding

The authors have nothing to report.

Conflicts of Interest

The authors declare no conflicts of interest.

Data Availability Statement

The data that support the findings of this study are available from the corresponding author upon reasonable request.

References

1. L. Ge, J. Li, L. Hou, and J. Lai, "Autonomous Voltage Regulation for Smart Distribution Network With High-Proportion PVs: A Graph Meta-Reinforcement Learning Approach," *IEEE Transactions on Sustainable Energy* 16, no. 4 (2025): 2768–2781, https://doi.org/10.1109/tste.2025.3566469.

2. U.S. Energy Information Administration, *Annual Energy Outlook 2025*. Report (U.S. Energy Information Administration, 2025): [Online], https://www.eia.gov/outlooks/aeo/.

3. V. Vijayan, A. Mohapatra, S. Singh, and C. L. Dewangan, "An Efficient Modular Optimization Scheme for Unbalanced Active Distribution Networks With Uncertain EV and PV Penetrations," *IEEE Transactions on Smart Grid* 14, no. 5 (2023): 3876–3888, https://doi.org/10.1109/tsg.2023.3234551.

4. International Energy Agency, *Global EV Outlook 2025* (International Energy Agency, 2025): [Online], https://www.iea.org/reports/global-ev-outlook-2025.

5. S. Islam, S. M. Muyeen, A. Iqbal, F. I. Bakhsh, and L. Ben-Brahim, "Effect of Battery Storage Based Electric Vehicle Chargers on Harmonic Profile of Power System Network, Current Scenario and Future Scope," *Journal of Energy Storage* 131 (2025): 117563, https://doi.org/10.1016/j.est.2025.117563.

6. G. Valverde and T. Van Cutsem, "Model Predictive Control of Voltages in Active Distribution Networks," *IEEE Transactions on Smart Grid* 4, no. 4 (2013): 2152–2161, https://doi.org/10.1109/tsg.2013.2246199.

7. Y. Li, Y. Su, Y. Zhang, W. Wu, and L. Xia, "Multiple-Time-Scale Scheduling by Optimizing the Degradation Cost Models of Hybrid Energy Storage Systems in Microgrids," *Energy Conversion and Management* 343 (2025): 120186, https://doi.org/10.1016/j.enconman.2025.120186.

8. O. Stanojev, Y. Guo, and G. Hug, "Online Feedback Droop Scheduling in Distribution Grids for Frequency and Local Voltage Control," *IEEE Transactions on Power Systems* 40, no. 5 (2025): 4105–4118, https://doi.org/10.1109/tpwrs.2025.3528752.

9. Q. Hou, N. Dai, and Y. Huang, "Voltage Regulation Enhanced Hierarchical Coordinated Volt/Var and Volt/Watt Control for Active Distribution Networks With Soft Open Points," *IEEE Transactions on Sustainable Energy* 15, no. 3 (2024): 2021–2037, https://doi.org/10.1109/tste.2024.3394049.

10. J. Xu, Y. Mu, W. Cheng, et al., "A Distributed Robust Voltage Control Framework for Active Distribution Systems," *IEEE Transactions on Industry Applications* 61, no. 2 (2025): 1896–1906, https://doi.org/10.1109/tia.2025.3532240.

11. R. S. Sutton and A. G. Barto, *Reinforcement Learning: An Introduction*. 1st ed. (MIT Press, 1998).

12. J. G. Vlachogiannis and N. D. Hatziargyriou, "Reinforcement Learning for Reactive Power Control," *IEEE Transactions on Power Systems* 19, no. 3 (2004): 1317–1325, https://doi.org/10.1109/tpwrs.2004.831259.

13. A. Bosisio, F. Soldan, M. Pisani, E. Bionda, F. Belloni, and A. Morotti, "A Q-Learning Algorithm for Optimizing on-Load Tap Changer Operation and Voltage Control in Distribution Networks With High Integration of Renewable Energy Sources," *Journal of Modern Power Systems and Clean Energy* 13, no. 6 (2025): 2063–2073, https://doi.org/10.35833/MPCE.2024.000528.

14. D. Cao, J. Zhao, W. Hu, F. Ding, Q. Huang, and Z. Chen, "Attention Enabled Multi-Agent DRL for Decentralized Volt-VAR Control of Active

Distribution System Using PV Inverters and SVCs," *IEEE Transactions on Sustainable Energy* 12, no. 3 (2021): 1582–1592, https://doi.org/10.1109/tste.2021.3057090.

15. J. Zhang, C. Lu, J. Si, J. Song, and Y. Su, "Deep Reinforcement Learning for Short-Term Voltage Control by Dynamic Load Shedding in China Southern Power Grid," in *2018 International Joint Conference on Neural Networks (IJCNN)* (IEEE, 2018), 1–8.

16. R. Diao, Z. Wang, D. Shi, Q. Chang, J. Duan, and X. Zhang, "Autonomous Voltage Control for Grid Operation Using Deep Reinforcement Learning," in *2019 IEEE Power & Energy Society General Meeting (PESGM)* (IEEE, 2019), 1–5.

17. Y. Deng, R. Paul, and Y.-J. Choi, "Multiple QoS Enabled Intelligent Resource Management in Vehicle-to-Vehicle Communication," *IEEE Transactions on Intelligent Transportation Systems* 25, no. 9 (2024): 12081–12094, https://doi.org/10.1109/tits.2024.3365557.

18. P. Kou, D. Liang, C. Wang, Z. Wu, and L. Gao, "Safe Deep Reinforcement Learning-based Constrained Optimal Control Scheme for Active Distribution Networks," *Applied Energy* 264 (2020): 114772, https://doi.org/10.1016/j.apenergy.2020.114772.

19. Y. Zhuang, F. Liu, Y. Huang, et al., "A Multiport DC Solid-State Transformer for MVDC Integration Interface of Multiple Distributed Energy Sources and DC Loads in Distribution Network," *IEEE Transactions on Power Electronics* 37, no. 2 (2021): 2283–2296, https://doi.org/10.1109/TPEL.2021.3105528.

20. Z. Zhang, H. Zhao, S. Fu, J. Shi, and X. He, "Voltage and Power Balance Control Strategy for Three-Phase Modular Cascaded Solid Stated Transformer," in *2016 IEEE Applied Power Electronics Conference and Exposition (APEC)* (IEEE, 2016), 1475–1480.

21. S. Madhusoodhanan, K. Mainali, A. Tripathi, et al., "Harmonic Analysis and Controller Design of 15 kV SiC IGBT-Based Medium-Voltage Grid-Connected Three-Phase Three-Level NPC Converter," *IEEE Transactions on Power Electronics* 32, no. 5 (2016): 3355–3369, https://doi.org/10.1109/tpel.2016.2582803.

22. A. B. Kunya, A. Nasir, and M. B. Garba, "Assessment of the State-of-the-Art of Solid-State Transformer Technology: Design, Control and Application," *Structure* 3, no. 1 (2024): 17–31, https://doi.org/10.59568/kjset-2024-3-1-02.

23. Y. Tahir, I. Khan, S. Rahman, et al., "A State-of-the-Art Review on Topologies and Control Techniques of Solid-State Transformers for Electric Vehicle Extreme Fast Charging," *IET Power Electronics* 14, no. 9 (2021): 1560–1576, https://doi.org/10.1049/pel2.12141.

24. J. Shi, W. Yang, F. Xue, W. Qiao, and D. Zhang, "Reactive Power Optimization of an Active Distribution Network Including a Solid State Transformer Using a Moth Swarm Algorithm," *Journal of Renewable and Sustainable Energy* 11, no. 3 (2019): 035501, https://doi.org/10.1063/1.5072789.

25. A. Bokhari, A. Alkan, R. Dogan, et al., "Experimental Determination of the ZIP Coefficients for Modern Residential, Commercial, and Industrial Loads," *IEEE Transactions on Power Delivery* 29, no. 3 (2013): 1372–1381, https://doi.org/10.1109/tpwrd.2013.2285096.

26. A. Ahmed, M. F. Nadeem, A. T. Kiani, N. Ullah, M. A. Khan, and A. Mosavi, "An Improved Hybrid Approach for the Simultaneous Allocation of Distributed Generators and Time Varying Loads in Distribution Systems," *Energy Reports* 9 (2023): 1549–1560, https://doi.org/10.1016/j.egyr.2022.11.171.

27. NREL, "Wind Resource Maps and Data," National Renewable Energy Lab, https://www.nrel.gov/gis/wind-resource-maps.html.

28. M. Rastegar, M. Fotuhi-Firuzabad, H. Zareipour, and M. Moeini-Aghtaieh, "A Probabilistic Energy Management Scheme for Renewable-Based Residential Energy Hubs," *IEEE Transactions on Smart Grid* 8, no. 5 (2016): 2217–2227, https://doi.org/10.1109/tsg.2016.2518920.

29. H. Aalami, M. P. Moghaddam, and G. R. Yousefi, "Modeling and Prioritizing Demand Response Programs in Power Markets," *Electric Power Systems Research* 80, no. 4 (2010): 426–435, https://doi.org/10.1016/j.epsr.2009.10.007.

30. J. Salehi and A. Abdolahi, "Optimal Scheduling of Active Distribution Networks With Penetration of PHEV Considering Congestion and Air Pollution Using DR Program," *Sustainable Cities and Society* 51 (2019): 101709, https://doi.org/10.1016/j.scs.2019.101709.

31. I. Goodfellow, Y. Bengio, and A. Courville, *Deep Learning* (MIT press, 2016).